AIP | Journal of Applied Physics

Electronic structure of CuCrO2 thin films grown on Al2O3(001) by oxygen plasma assisted molecular beam epitaxy

D. Shin, J. S. Foord, R. G. Egdell, and A. Walsh

Citation: J. Appl. Phys. **112**, 113718 (2012); doi: 10.1063/1.4768726
View online: http://dx.doi.org/10.1063/1.4768726
View Table of Contents: http://jap.aip.org/resource/1/JAPIAU/v112/i11
Published by the American Institute of Physics.

JOURNAL OF APPLIED PHYSICS **112**, 113718 (2012)

Electronic structure of $CuCrO_2$ thin films grown on Al_2O_3(001) by oxygen plasma assisted molecular beam epitaxy

D. Shin,[1] J. S. Foord,[1] R. G. Egdell,[1,a)] and A. Walsh[2]
[1]*Department of Chemistry, University of Oxford, Chemistry Research Laboratory, Mansfield Road, Oxford OX1 3TA, United Kingdom*
[2]*Centre for Sustainable Chemical Technologies and Department of Chemistry, University of Bath, Claverton Down, Bath BA2 7AY, United Kingdom*

(Received 22 August 2012; accepted 7 November 2012; published online 12 December 2012)

Thin films of $CuCrO_2$ have been grown on Al_2O_3(001) substrates by oxygen plasma assisted molecular beam epitaxy. With a substrate temperature of 700 °C or 750 °C, the films showed an unanticipated (015) orientation but at a higher substrate temperature of 800 °C the expected basal (001) orientation predominates. The optical absorption spectrum of $CuCrO_2$ shows a direct allowed absorption onset at 3.18 eV together with a weak peak at 2.0 eV which is suppressed by Sn doping. This suggests that the low energy peak should be attributed to 3d→3d excitations associated with Cu^{2+} defect states rather than excitations localised on Cr^{3+}. Valence band X-ray photoemission spectra of (001) and (015) oriented $CuCrO_2$ are compared with those obtained from polycrystalline samples. © *2012 American Institute of Physics*. [http://dx.doi.org/10.1063/1.4768726]

I. INTRODUCTION

Transparent conducting oxides (TCOs) combine the properties of optical transparency in the visible region with a high electrical conductivity.[1–3] They already find widespread application as a transparent electrode in display devices of various sorts and in many designs of solar cell. However, there is a growing interest in development of transparent electronic devices such as p-n junctions, transistors, and heterojunction lasers. These applications demand the availability of p-type TCOs to complement existing well established n-type materials, typified by ZnO, In_2O_3, and SnO_2. Despite ongoing reports of p-type doping in ZnO[4–7] and In_2O_3,[8,9] the realisation of p-type material is at best controversial and theoretical considerations suggest that reproducible p-type bulk doping is probably impossible.[10,11] These limitations have led to interest in p-type TCOs based on 3 d[10] Cu(I). The parent oxide Cu_2O is well known as a p-type material but the intrinsic band gap of 2.17 eV (Refs. 12 and 13) is too small for application as a TCO. Hosono and co-workers devised a general principal for design of Cu(I) TCOs based on reduced dimensionality in the interaction between adjacent Cu(I) sites as compared to Cu_2O. The first compound to be developed in this way was the delafossite oxide $CuAlO_2$,[14] followed later by $CuGaO_2$[15] and $SrCu_2O_2$.[16]

$CuCrO_2$ has been the object of recent interest as a further *p*-type TCO. It remains tolerably transparent in the visible region despite the fact that there must be dipole forbidden 3 *d*→3 *d* excitations centered on Cr in the visible region. Hole mobilities of 11 $cm^2\ V^{-1}\ s^{-1}$ have been measured with carrier concentrations around $4.75 \times 10^{17}\ cm^{-3}$ in thin-film material doped by native defects.[17] Higher levels of *p*-type doping can be achieved by substitution of Cr^{3+} with divalent cations. Mg-doped $CuCrO_2$ has the highest reported *p*-type conduction of any TCO.[18] Other divalent dopants such as Ca,[19] Ni,[20] and Cd[21] have also been studied.

The focus on $CuCrO_2$ as an optimal p-type transparent conducting oxide has led to an upsurge of interest in growing thin films of the material. Pulsed laser deposition has been the most popular growth technique,[15,22–25] but thin films have also been prepared by chemical vapour deposition[17] and sol gel techniques.[26,27] Basal plane alumina, i.e., Al_2O_3(001) has proved to be the most popular single crystal substrate for attempted epitaxial growth and has been shown to promote growth of (001) oriented Al_2O_3. In the present contribution, thin films of $CuCrO_2$ are grown by molecular beam epitaxy (MBE). The focus of the paper is on the growth process and the electronic structure of the films. Optimisation of transport properties of MBE-grown material will be the subject of subsequent publications.

The rhombohedral (space group $R\bar{3}m$) delafossite structure of 3*R*-$CuCrO_2$ is based on trilayer sheets comprised of Cr ions occupying the octahedral holes between two close packed layers of O ions (Fig. 1). The O ions in the sheets are linked via linear O-Cu-O dumbbells. The Cr ions are arranged in an ABCABC stacking sequence: an alternative hexagonal polymorph (space group $P6_3/mmc$) based on ABAB stacking is also known giving 2*H*-$CuCrO_2$. Both polymorphs[28] can be described in terms of hexagonal cells, with $a = b = 2.970$ Å and $c = 11.400$ Å for the 2*H*-polymorph[29] and $a = b = 2.973$ Å and $c = 17.100$ Å for the 3*R*-polymorph.[30] The structure of α-alumina (corundum) is based on a hexagonally close packed array of oxygen ions with occupation of 2/3 of the octahedral holes between successive layers by aluminum ions. The structure belongs to the rhombohedral space group $R\bar{3}c$ but again the structure can be defined in terms of a hexagonal cell with $a_s = b_s = 4.759$ Å and $c_s = 12.991$ Å (here the subscript *s* designates substrate). The average O-O separation in the close packed layers is $a_s/\sqrt{3} = 2.748$ Å. There is thus a large mismatch of 8.2%

a)Author to whom correspondence should be addressed. Electronic mail: Russell.egdell@chem.ox.ac.uk.

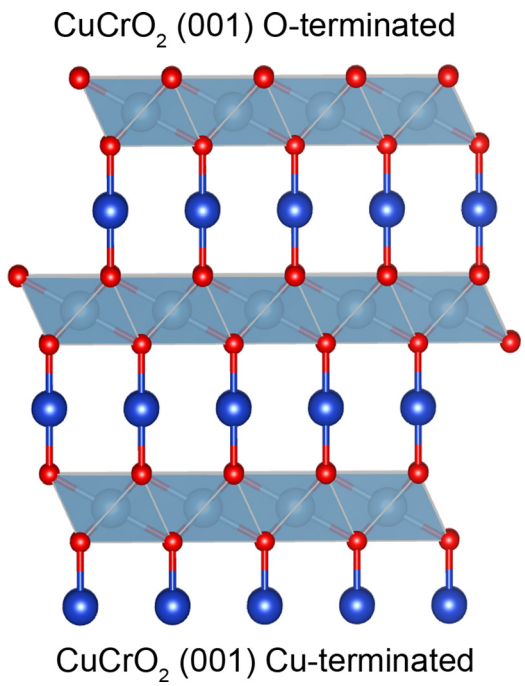

FIG. 1. Crystal structure of the 3*R*-polymorph of $CuCrO_2$. Oxygen ions are small spheres (red online), copper ions large spheres (dark blue online), and chromium large spheres within shading (light blue online). The CrO_6 octahedra are shaded.

between the O-O separations in $CuCrO_2$ and Al_2O_3, with the $CuCrO_2$ under compressive stress.

In the present paper, thin films of $CuCrO_2$ are grown on c-plane (i.e., 001) Al_2O_3. At a substrate temperature of 800 °C (001) oriented films are obtained as expected. However, at a lower substrate temperature of 700 °C, an unanticipated (015) orientation was found. This can, however, be rationalized by consideration of the interfacial structure and simple estimates of surface energies based on densities of dangling bonds. Photoemission spectra were measured for both terminations and the valence band spectra were shown to exhibit significant differences.

II. EXPERIMENTAL PROCEDURE

$CuCrO_2$ films were grown on 1 cm × 1 cm Al_2O_3(001) substrates (PiKem, UK) in an ultrahigh vacuum oxide MBE system (SVT, USA) with a base pressure of 5×10^{-10} mbar. This incorporated high temperature Cr and Cu effusion cells and a radio frequency (RF) plasma oxygen atom source operated at 200 W RF power with an oxygen background pressure of 2×10^{-5} mbar. Substrates were heated radiatively using a graphite filament. The Al_2O_3 substrates were cleaned by exposure to the oxygen atom beam at a substrate temperature of 850 °C. Growth runs were carried out with substrate temperatures between 700 °C and 800 °C as measured by a thermocouple located close behind the substrate. It was established empirically that single phase (as gauged by x-ray diffraction) 3*R*-$CuCrO_2$ could be grown at a rate of around 0.2 nm/s with cell temperatures of 1100 °C for Cu and 1500 °C for Cr, provided that growth was seeded by deposition of a layer of Cu (again with 1100 °C cell temperature but in the absence of the O plasma) during a 270 s deposition. Following growth of the $CuCrO_2$ layer for a further 1800 s, films were post-annealed at the growth temperature for 10 min to allow for interdiffusion of the layers. As well as ensuring the correct stoichiometry, this two step growth process also minimized the inclusion of oxidized Cu(II) in the films.

Films were characterized by x-ray diffraction (XRD), atomic force microscopy (AFM), x-ray photoelectron spectroscopy (XPS), and optical absorption spectroscopy. High resolution XRD θ–2θ measurements were performed on a Philips Xpert diffractometer using monochromatic CuKα radiation ($\lambda = 1.5406$ Å). High-resolution x-ray photoemission spectra were measured in a Scienta ESCA 300 spectrometer. This incorporates a rotating anode Al $K\alpha$ ($h\nu = 1486.6$ eV x-ray source), a seven-crystal x-ray monochromator, and a 300 mm mean radius spherical sector electron energy analyzer with parallel electron detection system. The x-ray source was ran with 200 mA emission current and 14 kV anode bias, while the analyzer operated at 150 eV pass energy. Gaussian convolution of the analyzer resolution with a linewidth of 260 meV for the x-ray source gives an effective instrument resolution of 400 meV. Samples were cleaned *in situ* by annealing at 400 °C. The C 1*s* to O 1*s* intensity ratio was reduced to below 1/100. Binding energies are referenced to the Fermi energy of a silver sample regularly used to calibrate the spectrometer.

III. RESULTS AND DISCUSSION

θ–2θ x-ray diffraction profiles of $CuCrO_2$ grown at different temperatures are shown in Fig. 2. With a substrate temperature of 800 °C, the dominant reflections from the epilayer are associated with the (00$\underline{3}$n) Bragg peaks (n = 1,2,3,4), with the (006) reflection strongest. Thus the expected growth mode with the c-axis of the epilayer normal to the surface is realized. However, a very weak (015) reflection close to the substrate (006) reflection is just discernible with an intensity a factor of 50 lower than the epilayer (006) peak. This peak becomes stronger at lower growth temperatures and for a sample grown at 700 °C there is almost perfect (015) texture in the epilayer, with the (006) reflection a factor of ~500 weaker than the (015) reflection. No other orientations are present for films grown at both low and high temperatures. Interestingly, the full width at half maximum height for the strongest epilayer peak is lower for the (015) sample grown at 700 °C than for the (001) sample grown at 800 °C (Fig. 2 right hand panels). Samples grown at both temperatures showed a rough surface morphology, as gauged by AFM (Fig. 3). The (001) sample exhibited surface blocks with a reasonably uniform size distribution, characterized by lateral dimensions just below 200 nm. Grain growth was more pronounced on the (015) surface with surface domains up to about 500 nm in size, although much smaller grains were found between the largest ones. Despite the narrower diffraction peaks, the (015) surface was much rougher (Fig. 3). The overwhelming predominance of the (00 n) reflections in samples grown at 800 °C and the near perfect (015) texture for samples grown at 700 °C is somewhat surprising given the granular appearance of the films and suggests that a columnar growth mode must pertain.

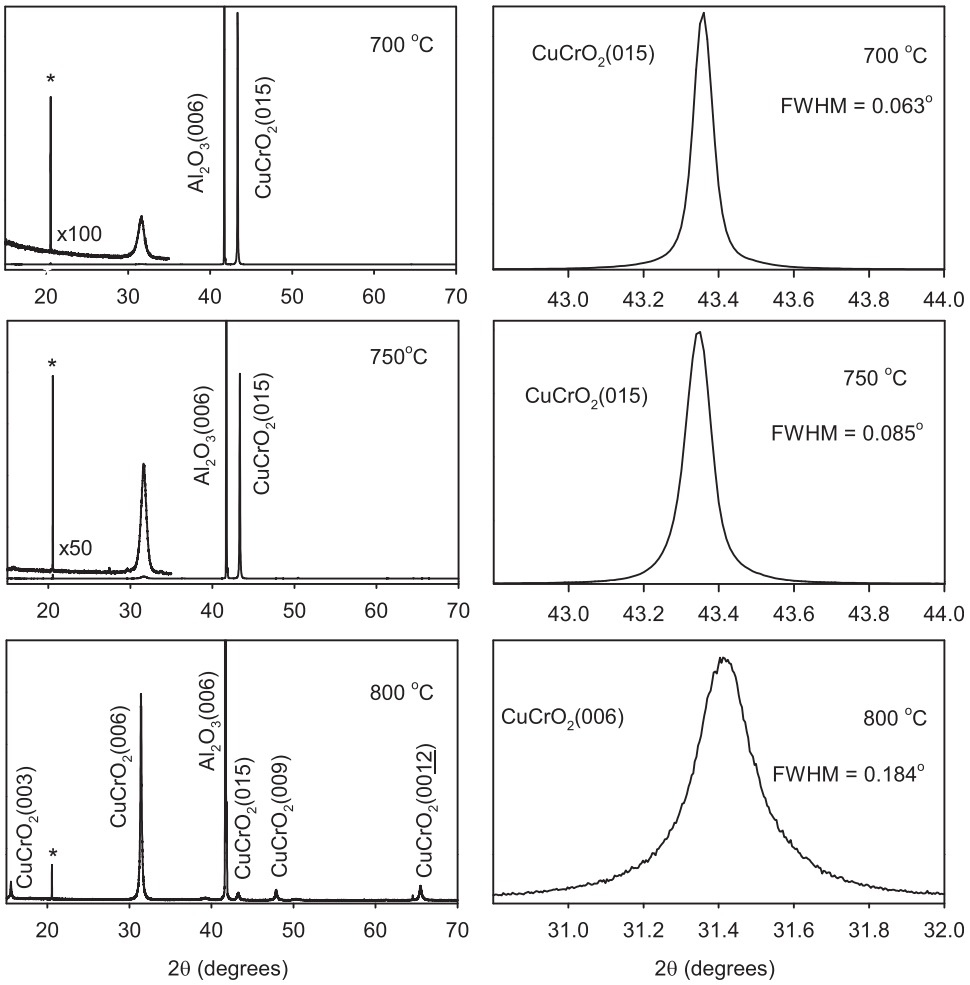

FIG. 2. Left hand panels: θ–2θ X-ray diffraction profiles for $CuCrO_2$ films grown at the substrate temperatures indicated. The feature marked by * is a secondary diffraction peak from the substrate. Right hand panels: expanded θ–2θ X-ray diffraction profiles across the strongest epilayer reflection for the $CuCrO_2$ thin films.

The stability of the (015) surface can be rationalized by very simple structural and energetic considerations. A side view the (015) oriented delafossite structure is shown in Fig. 4 along with a similar view of the (001) O-terminated surface of Al_2O_3. Top views are also shown. The (001) termination shown in Fig. 1 involves cutting one Cu-O bond per rhombic surface unit cell ($a = b = 2.973$ Å, $\gamma = 60°$, area 7.656 Å^2) to give either a Cu or O terminated polar surface. As will emerge below, alternative terminations that involve cutting 3 Cr-O bonds per cell are unlikely on the basis of simple energetic considerations. The (015) surface involves cutting two Cr-O bonds and one Cu-O bond in a larger rhomboidal surface unit cell whose sides are defined by edges of length a and e ($a = 2.973$ Å, $e = 7.431$ Å, $\gamma = 78.46°$, area 21.65 Å^2). Two complementary polar terminations are then possible. The first has stoichiometry CrO_2 and involves stripes of edge sharing CrO_4 plaquettes running along a [100] direction with single dangling bonds on one Cr and one O per cell pointing roughly normal to the surface, together with a single dangling bond on O pointing obliquely to the surface. The complementary termination involves an outer layer of Cu atoms each with a single dangling bond oblique to the surface normal, together with normally oriented dangling bonds on one Cr and one O per cell. Using bulk thermochemical data[31] for Cu_2O and Cr_2O_3, we can estimate that the energy associated with cutting a single Cu-O bond for two coordinate Cu(I) is 274 kJ/mole, as compared to 223 kJ/mole for a single Cr-O bond for 6-coordinate Cr(III). In this way, we can make rough estimates of the unrelaxed surface energies for the (001) and (015) terminations. These turn out to be, respectively, 2.97 J m^{-2} for the (001) surface and 2.76 J m^{-2} for the (015) surface. Bearing in mind that there must be very pronounced surface relaxation, it can be seen that the surface energies are finely balanced. Moreover, the separation d between rows of Cu or Cr ions on the (015) surfaces is equal to $b \times \sin(78.46°)$ which is 7.280 Å. It emerges that d is roughly equal to $3 \times a_s/2 = 7.138$ Å, i.e., three times the distance between adjacent rows of O ions on the O-terminated (001) surface of Al_2O_3. As mentioned previously the cation periodicity along $\langle 100 \rangle$ directions in the epilayer have a mismatch of 8.2% with the periodicity in oxygen positions on the Al_2O_3(001) surface, but in the orthogonal direction the mismatch in inter-row separations is only 1.99%. This allows construction of schematic interface structures with reasonable matching of atomic positions at the interface, as shown schematically in Fig. 5. For the (001) termination of $CuCrO_2$, the 11.2% mismatch pertains in two high symmetry in-plane directions. These considerations help to explain the unanticipated appearance of an (015) oriented epilayer during growth at 700 °C. Clearly, it would be desirable to perform more rigorous calculations of surface energies; however, this is complicated by the inherently polar nature of any stoichiometric termination.

The optical absorption spectrum of $CuCrO_2$ is shown in Fig. 6 as a plot of absorption coefficient α against photon

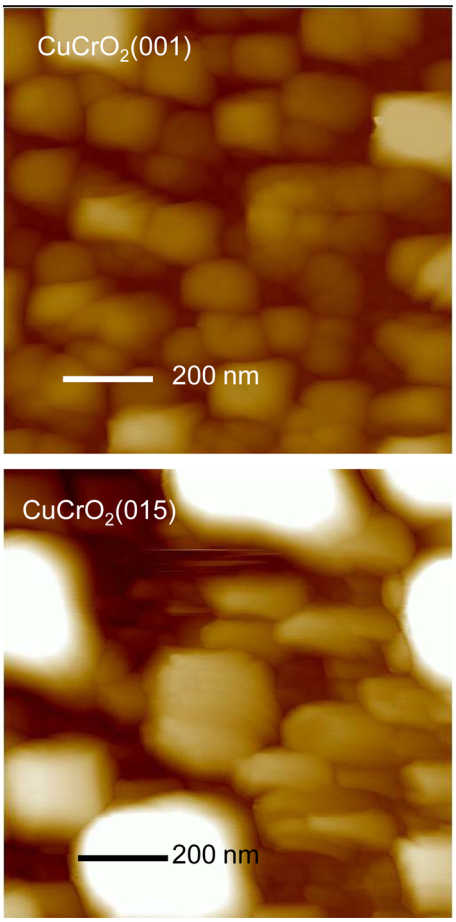

FIG. 3. 1 μm × 1 μm AFM images of (001) and (015) oriented $CuCrO_2$ thin films. The height range is 200 nm in each case and the root mean square roughnesses are, respectively, 30 nm and 50 nm.

energy hν. In agreement with Hiraga *et al.*,[32] we find a well-defined absorption maximum at about 3.6 eV. This is attributed to transitions from the peak in the occupied Cu 3d partial density of states into hybridized Cu $3dz^2 + 4s$ states—Van Hove singularities are found in both the occupied and empty density of states due to the effective low dimensionality of the delafossite structure, giving rise to a relatively well defined absorption peak. From a plot of the $(\alpha h\nu)^2$ against photon energy for the leading edge of this peak, we find a value for the direct allowed bandgap of just under 3.2 eV, in agreement with values found elsewhere. However, it is clear that a tail of weak absorption extends to lower energy and, in addition, a weak but well defined peak is found at around 2.02 eV. Recent theoretical work suggests that as with the other delafossites, the lowest energy band gap in 2*H*-$CuCrO_2$ is indirect with a separation between the lowest energy direct and indirect gaps of about 0.5 eV at the GGA + U level of theory[33] but only 0.2 eV using a screened exchange approach.[34] Taking these numbers in conjunction with the experimental direct gap of 3.18 eV gives alternative estimates of 2.68 eV or 2.98 eV for the lowest energy indirect gap. Thus forbidden or indirect interband transitions may account for the weak absorption tail just below 3 eV if we take the GGA + U estimate, but do not account for the peak at 2.02 eV. We note in passing that indirect gaps, as low as 1.28 eV (Ref. 35) or 1.45 eV, have been suggested on the basis of earlier[17] experimental work but such low energies are inconsistent with calculations.

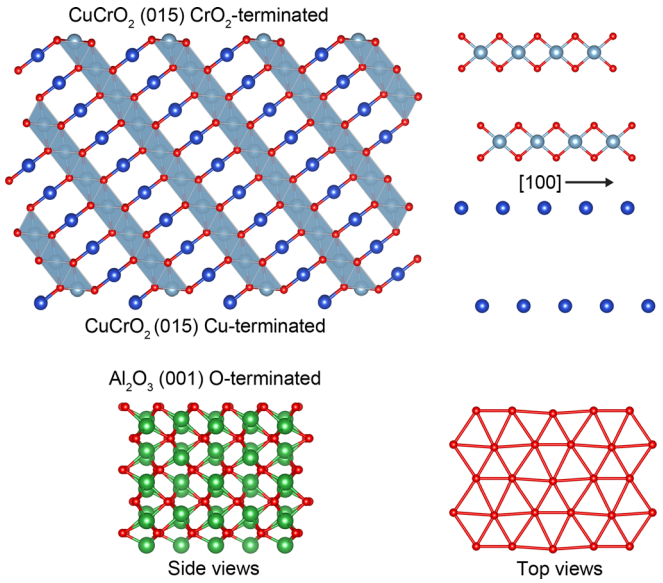

FIG. 4. Upper panels. Left: side views of the CrO_2 and Cu (015) terminations of $CuCrO_2$. Right: top views of the two terminations showing only the ions in the outermost ionic plane. Coding is as in Figure 1. Lower panels. Left: side view of the O-terminated surface of Al_2O_3(001). Oxygen ions are small spheres (red online), aluminium ions are large spheres (green online). Right: top view of the (001) termination of Al_2O_3.

This leads us to consider the role of low energy localized 3*d* to 3*d* excitations. Two types of localised transition need to be considered. First, $3d^3$ Cr^{3+} ions in an O_h environment possesses a $^4A_{2g}$ ground state associated with the t_{2g}^3 configuration with low lying $^4T_{2g}$ and $^4T_{1g}$ exited states derived from the $t_{2g}^2e_g^1$ configuration. Excitations to these two states are found at 2.08 eV and 2.64 eV, respectively,[36] in Cr_2O_3 so that assignment of the absorption at 2.02 eV to $^4A_{2g} \rightarrow {}^4T_{2g}$ excitation seems plausible, although on the basis of resonant inelastic X-ray scattering it has been suggested that the $^4A_{2g} \rightarrow {}^4T_{1g}$ excitation occurs at a slightly lower energy of 2.1 eV in $CuCrO_2$ itself (as compared to 2.64 eV in Cr_2O_3).[37] More significantly, the 2 eV peak is also found for films of $CuGaO_2$ and in both systems the peak is absent in samples doped with Sn. This leads us to suggest

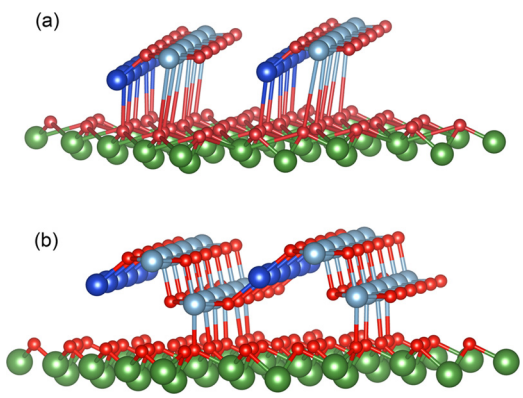

FIG. 5. Two possible interface structures for $CuCrO_2$(015) on Al_2O_3(001). (a) For Cu terminated $CuCrO_2$(015) surface (b) for CrO_2 terminated $CuCrO_2$(015) surface.

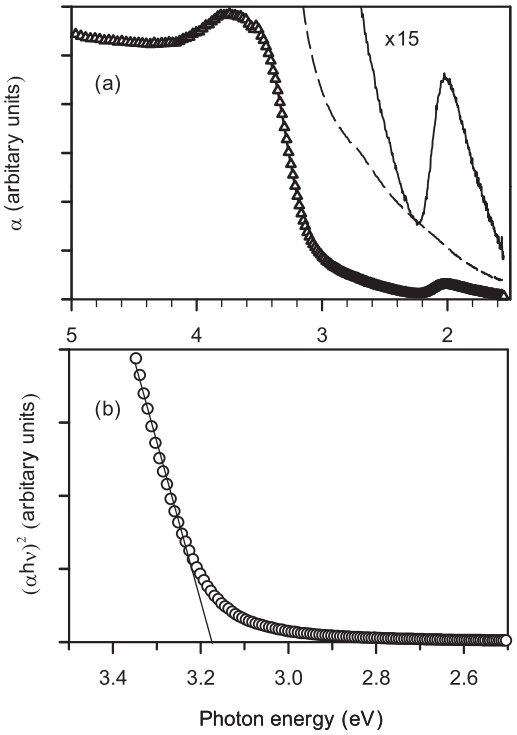

FIG. 6. (a) Absorption spectrum of (001) oriented $CuCrO_2$ thin film presented in a plot of absorption coefficient α against photon energy $h\nu$. The low energy region is expanded to show a peak at 2 eV. The dashed line is the absorption spectrum in the low energy region from a sample incorporating 5% Sn dopant. (b) Expansion of the band edge region in a plot of $(\alpha h\nu)^2$ versus photon energy $h\nu$ used to determine the direct allowed absorption onset.

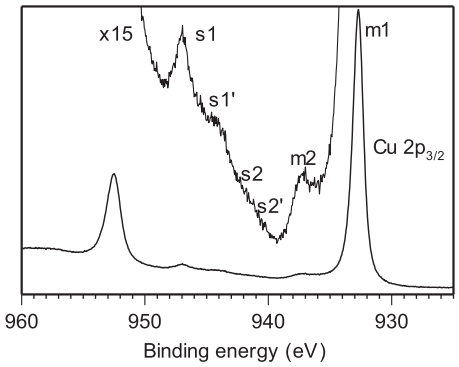

FIG. 7. XPS of $CuCrO_2$(001) in Cu 2p core level region.

that the low energy absorption is associated with Cu^{2+} defect states arising from cation deficiency: recent theoretical work suggests that cation vacancies are likely to be the dominant native defect in copper delafossites.[38] Sn^{4+} on Cr^{3+} (or Ga^{3+}) sites will act as an n-type donor able to compensate p-type Cu^{2+} acceptor states. This hypothesis requires one to assume both that the two dipole forbidden excitations localised on Cr^{3+} are too weak to be observed in absorption spectra of thin films or are buried under the indirect absorption onset; and that defect related Cu^{2+} excitations are more intense. This latter condition in turn implies that that the inversion symmetry found for the bulk Cu^{+} sites is absent for Cu^{2+} defect sites, so that transitions are no longer parity forbidden. Further theoretical work is needed to clarify these ideas.

Core level XPS confirms the presence of Cu^{2+} defect states, at least in the near-surface region probed by the technique. Fig. 7 shows the spectrum of a $CuCrO_2$ thin film in the region of the Cu $2p_{3/2}$ core level. The Cu 2*p* spectra are dominated by a simple spin-orbit split doublet. The $2p_{3/2}$ component labelled m1 in Fig. 4 is found at 932.7 eV binding energy and has a full width at half maximum of 0.99 eV. This corresponds to a Cu $2p^5 3d^{10}$ configuration in the final state arising from the dominant Cu(I) initial state. A series of satellite peaks and shoulders labelled s1, s1′, s2, s2′, and m2 are observed between the main $2p_{3/2}$ and $2p_{1/2}$ peaks. Moving left to right in the spectrum, s1 and s1′ correspond to structure arising from $3d^9$ final states associated with $3d^{10}$ Cu(I) in the initial state. The appearance of these peaks requires interband shake-up excitation into the empty conduction band which is of dominant Cu 4*s*/Cu 4*p* character.[39] Thus the formal configuration is Cu $2p^5\ 3d^9\ (4s4p)^1$. The shoulders s2 and s2′ are poorly defined in the current spectrum (but more obvious in previously published spectra of $CuAlO_2$).[40] This structure arises from $3d^9$ Cu(II) in the initial state giving rise to unscreened Cu $2p^5 3d^9$ final states and appears at lower binding energy than s1 and s1′ because no interband excitation is required to realise a Cu $2p^5 3d^9$ final state. Finally, the weak but well-defined peak m2 is to be assigned to a Cu $2p^5 3d^{10}$ final state associated with Cu(II) $3d^9$ in the initial state. The core hole potential lowers the energy of the $3d^9$ level below that of the oxygen valence levels and realisation of a $3d^{10}$ final state involves local screening by charge transfer from the O 2*p* states to give a final state configuration Cu $2p^5 3d^{10}$ O $2p^5$. A non-local screening channel[41–43] where the valence band hole delocalizes away from the ionized site to give Zhang-Rice singlet states is not possible when the Cu sites have no connectivity with each other, as is the case for a defect Cu(II) ion constrained within the delafossite structure. The local screening channel also dominates in oxides such as Li_2CuO_2, where square CuO_4 plaquettes are connected through Cu-O-Cu linkages with a bond angle of 90°.[44,45] The binding energy of 937.2 eV found for $CuCrO_2$ is very similar to that of 937.1 eV for $CuAlO_2$ but is much higher than the value of 934.0 eV for Li_2CuO_2.[44,45] The binding energy is determined by the Coulombic interaction between the Cu 2*p* core level and the O 2*p* valence hole. This interaction should be much stronger in $CuCrO_2$ than in Li_2CuO_2 due to the lower coordination number and shorter Cu-O bond lengths: in $CuCrO_2$, the Cu-O bond length is only 1.86 Å whereas in Li_2CuO_2 the bond length is 1.96 Å. Thus the unusual screened final structure associated with Cu(II) defect states in Cu(I) delafossites is a consequence of the Cu(II) ions being constrained to an unusual linear coordination site.

Valence region x-ray photoemission spectra of $CuCrO_2$(001) and $CuCrO_2$(015) are shown in Fig. 8, with the spectrum of a polycrystalline sample overlaid. The lower panel shows the cross section weighted partial densities of states adapted from the publication of Arnold *et al.*[37] There is generally good correspondence between the two experimental spectra and the calculations. In each case, it is

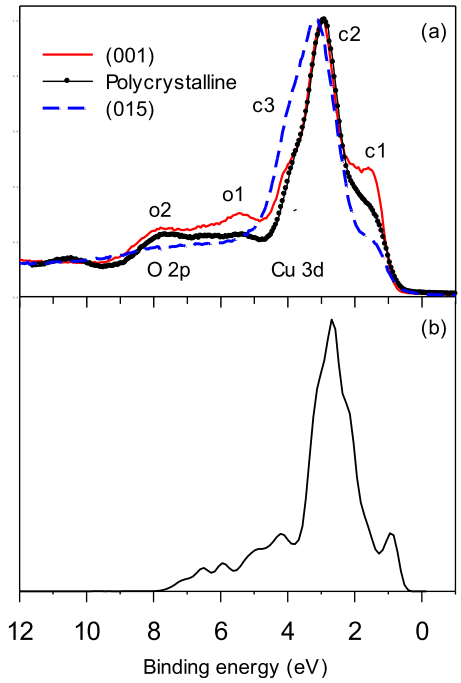

FIG. 8. (a) Valence band XPS for $CuCrO_2$(001) and $CuCrO_2$(015). The experimental spectrum for polycrystalline $CuCrO_2$ is also shown. (b) Cross section weighted density of states for $CuCrO_2$ adapted from Ref. 37.

possible to discern 5 main features in the spectra. There is a dominant peak labeled c2, which has two shoulders c1 and c3 on the low and high binding energy sides—c1 is generally better defined than c3. At higher binding energy, there are two much weaker features labeled o1 and o2. The three features c1-c3 relate to states of dominant Cu 3*d* atomic character which in the linear environment of the delafossite structure are split into state of local σ, π, and δ symmetry.[46] The two features o1 and o2 derive from states of dominant O 2p atomic character. There is very pronounced covalent mixing between Cu 3*d* and O 2*p* states. Moreover, the Cu 3d one electron ionization cross section at 1486.6 eV photon energy is around a factor of 20 bigger than the corresponding O 2*p* cross section,[40,47] so that the spectrum in what is nominally the O 2*p* region is in fact dominated by covalent hybridization with Cu 3*d* states.

Significant differences between the spectra of the (001) and (015) oriented samples may be noted. First, the intensity of the Cu 3*d* related structure (c1-c3) relative to the O 2*p* structure (o1-o2) is bigger for the (015) film than for the (001) film. Data for the polycrystalline sample are intermediate between the two. This observation is consistent with an O-terminated surface for $CuCrO_2$(001) formed by cleavage of O-Cu bonds, with the first Cu ions located about 3.8 Å below the outer O layer. The Cu ions are about 1.0 Å below the cut which generates the CrO_2 terminated (015) surface. The second major difference relates to intensity distribution within the Cu 3*d* bands. The low binding energy shoulder c1 is found to be much stronger relative to c2 and c3 for the (001) film than for the (015) film. This shoulder is much stronger for $CuCrO_2$ than for $CuAlO_2$ leading to the suggestion that it arises from hybridization of Cr 3*d* states with Cu 3*d* and O 2*p* states in the upper part of the valence band. The proposed model for the (001) surface obviously involves Cr ions immediately below the outer O layer.

Finally, it should be noted that for both film orientations the valence band edge lies very close to the Fermi level, as is expected for p-type materials where the Fermi level is pinned by states toward the bottom of the bulk band gap.

IV. CONCLUSIONS

In summary, highly oriented thin films of $CuCrO_2$ have been grown on Al_2O_3(001) by oxygen plasma assisted molecular beam epitaxy. With a substrate temperature of 800 °C, the expected (001) orientation was obtained but at lower temperatures an unanticipated (015) orientation predominated. Simple bond energy considerations suggest that the surface energies for these two orientations should be quite close to each other. On the other hand, (015) growth allows better matching of atomic positions at the interface than can be achieved for (001) films. Small but significant differences between valence band photoemission spectra for the two differently oriented surfaces may be rationalized in terms of the positions of Cu ions relative to the outer atomic layer of the surface.

ACKNOWLEDGMENTS

The Oxford MBE programme was supported by EPSRC Grant GR/S94148.

[1]C. G. Granqvist, Sol. Energy Mater. Sol. Cells **91**, 1529 (2007).
[2]D. S. Ginley and C. Bright, MRS Bull. **25**, 15 (2000).
[3]Handbook of Transparent Conductors, D. S. Ginley, H. Hosono, and D. C. Paine, eds. (Springer, New York, 2010).
[4]U. Ozgur, Y. I. Alivov, C. Liu, A. Teke, M. A. Reshchikov, S. Dogan, V. Avrutin, S. J. Cho, and H. Morkoc, J. Appl. Phys. **98**, 041301(2005).
[5]A. Tsukazaki, A. Ohtomo, T. Onuma, M. Ohtani, T. Makino, M. Sumiya, K. Ohtani, S. F. Chichibu, S. Fuke, Y. Segawa, H. Ohno, H. Koinuma, and M. Kawasaki, Nat. Mater. **4**, 42 (2005).
[6]S. J. Pearton, D. P. Norton, K. Ip, Y. W. Heo, and T. Steiner, Prog. Mater. Sci. **50**, 293 (2005).
[7]D. C. Look, D. C. Reynolds, C. W. Litton, R. L. Jones, D. B. Eason, and G. Cantwell, Appl. Phys. Lett. **81**, 1830 (2002).
[8]J. Stankiewicz, F. Villuendas, and R. Alcala, Appl. Phys. Lett. **96**, 192108 (2010).
[9]J. Stankiewicz, M. Pilar Lozano, and F. Villuendas, Phys. Rev. B **85**, 125306 (2012).
[10]S. B. Zhang, S. H. Wei, and A. Zunger, Phys. Rev. B **63**, 075205 (2001).
[11]J. Robertson, R. Gillen, and S. J. Clark, Thin Solid Films **520**, 3714 (2012).
[12]S. Nikitine, J. B. Grun, and M. Sieskind, J. Phys. Chem. Solids **17**, 292 (1961).
[13]J. B. Grun, M. Sieskind, and S. Nikitine, J. Phys. Chem. Solids **19**, 189 (1961).
[14]H. Kawazoe, M. Yasukawa, H. Hyodo, M. Kurita, H. Yanagi, and H. Hosono, Nature **389**, 939 (1997).
[15]K. Ueda, T. Hase, H. Yanagi, H. Kawazoe, H. Hosono, H. Ohta, M. Orita, and M. Hirano, J. Appl. Phys. **89**, 1790 (2001).
[16]H. Ohta, M. Orita, M. Hirano, K. Ueda, and H. Hosono, Int. J. Mod. Phys. B **16**, 173 (2002).
[17]S. Mahapatra and S. A. Shivashankar, Chem. Vap. Deposition **9**, 238 (2003).
[18]R. Nagarajan, A. D. Draeseke, A. W. Sleight, and J. Tate, J. Appl. Phys. **89**, 8022 (2001).
[19]H. Huang, C. F. Zhu, and W. Liu, Chinese J. Chem. Phys. **17**, 161 (2004).
[20]S. Y. Zheng, G. S. Jiang, J. R. Su, and C. F. Zhu, Mater. Lett. **60**, 3871 (2006).
[21]M. V. Lalic and J. Mestnik-Filho, J. Phys.-Condens. Matter **18**, 1619 (2006).

[22]D. Li, X. D. Fang, Z. H. Deng, S. Zhou, R. H. Tao, W. W. Dong, T. Wang, Y. P. Zhao, G. Meng, and X. B. Zhu, J. Phys. D-Appl. Phys. **40**, 4910 (2007).
[23]P. W. Sadik, M. Ivill, V. Craciun, and D. P. Norton, Thin Solid Films **517**, 3211 (2009).
[24]S. Y. Kim, S. Y. Sung, K. M. Jo, J. H. Lee, J. J. Kim, S. J. Pearton, D. P. Norton, and Y. W. Heo, J. Crystal Growth **326**, 9 (2011).
[25]D. Li, X. D. Fang, A. W. Zhao, Z. H. Deng, W. W. Dong, and R. H. Tao, Vacuum **84**, 851 (2010).
[26]Y. F. Wang, Y. J. Gu, T. Wang, and W. Z. Shi, J. Alloys Compd. **509**, 5897 (2011).
[27]Y. F. Wang, Y. J. Gu, T. Wang, and W. Z. Shi, J. Sol-Gel Sci. Technol. **59**, 222 (2011).
[28]O. Crottaz, F. Kubel, and H. Schmid, J. Solid State Chem. **122**, 247 (1996).
[29]O. Crottaz and F. Kubel, Z. Kristallogr. **211**, 481 (1996).
[30]O. Crottaz and F. Kubel, Z. Kristallogr. **211**, 482 (1996).
[31]M. Binnewies and E. Milke, *Thermochemical Data of Elements and Compounds*, 2nd ed. (Wiley-VCH Verlag GmBH, Weinheim, 2002).
[32]H. Hiraga, T. Makino, T. Fukumura, H. M. Weng, and M. Kawasaki, Phys. Rev. B **84**, 041411 (2011).
[33]D. O. Scanlon, A. Walsh, B. J. Morgan, G. W. Watson, D. J. Payne, and R. G. Egdell, Phys. Rev. B **79**, 035101 (2009).
[34]R. Gillen and J. Robertson, Phys. Rev. B **84**, 035125 (2011).
[35]F. A. Benko and F. P. Koffyberg, Mater. Res. Bull. **21**, 753 (1986).
[36]D. S. McClure, J. Chem. Phys. **38**, 2289 (1963).
[37]T. Arnold, D. J. Payne, A. Bourlange, J. P. Hu, R. G. Egdell, L. F. J. Piper, L. Colakerol, A. De Masi, P. A. Glans, T. Learmonth, K. E. Smith, J. Guo, D. O. Scanlon, A. Walsh, B. J. Morgan, and G. W. Watson, Phys. Rev. B **79**, 075102 (2009).
[38]D. O. Scanlon and G. W. Watson, J. Mater. Chem. **21**, 3655 (2011).
[39]K. Karlsson, O. Gunnarsson, and O. Jepsen, J. Phys. Condens. Matter **4**, 2801 (1992).
[40]D. J. Aston, D. J. Payne, A. J. H. Green, R. G. Egdell, D. S. L. Law, J. Guo, P. A. Glans, T. Learmonth, and K. E. Smith, Phys. Rev. B **72**, 195115 (2005).
[41]M. A. Vanveenendaal, H. Eskes, and G. A. Sawatzky, Phys. Rev. B **47**, 11462 (1993).
[42]M. A. Vanveenendaal and G. A. Sawatzky, Phys. Rev. Lett. **70**, 2459 (1993).
[43]T. Boske, K. Maiti, O. Knauff, K. Ruck, M. S. Golden, G. Krabbes, J. Fink, T. Osafune, N. Motoyama, H. Eisaki, and S. Uchida, Phys. Rev. B **57**, 138 (1998).
[44]K. Karlsson, O. Gunnarsson, and O. Jepsen, Int. J. Mod. Phys. B **14**, 3791 (2000).
[45]K. Karlsson, O. Gunnarsson, and O. Jepsen, Phys. Rev. Lett. **82**, 3528 (1999).
[46]D. Shin, J. S. Foord, D. J. Payne, T. Arnold, D. J. Aston, R. G. Egdell, K. G. Godinho, D. O. Scanlon, B. J. Morgan, G. W. Watson, E. Mugnier, C. Yaicle, A. Rougier, L. Colakerol, P. A. Glans, L. F. J. Piper, and K. E. Smith, Phys. Rev. B **80**, 233105 (2009).
[47]J. P. Hu, D. J. Payne, R. G. Egdell, P. A. Glans, T. Learmonth, K. E. Smith, J. Guo, and N. M. Harrison, Phys. Rev. B **77**, 155115 (2008).